

1 Quasi-weekly oscillation of regional PM_{2.5} transport over 2 China driven by the synoptic-scale disturbance of East 3 Asian Winter Monsoon circulation

4 Yongqing Bai ¹, Tianliang Zhao ^{2,*}, Kai Meng ^{3,*}, Yue Zhou ¹, Jie Xiong ¹, Xiaoyun
5 Sun ⁴, Lijuan Shen ⁵, Yanyu Yue ¹, Yan Zhu ¹, Weiyang Hu ⁶, Jingyan Yao ²

6 ¹China Meteorological Administration Basin Heavy Rainfall Key Laboratory/Hubei Key Laboratory
7 for Heavy Rain Monitoring and Warning Research, Institute of Heavy Rain, China Meteorological
8 Administration, Wuhan 430205, China

9 ²Climate and Weather Disasters Collaborative Innovation Center, Key Laboratory for
10 Aerosol-Cloud-Precipitation of China Meteorological Administration, Nanjing University of
11 Information Science & Technology, Nanjing 210044, China

12 ³Key Laboratory of Meteorology and Ecological Environment of Hebei Province, Hebei Provincial
13 Institute of Meteorological Sciences, Shijiazhuang, 050021, China

14 ⁴Anhui Province Key Laboratory of Atmospheric Science and Satellite Remote Sensing, Anhui Institute
15 of Meteorological Sciences, Hefei 230031, China

16 ⁵School of Atmosphere and Remote Sensing, Wuxi University, Wuxi, 214105, China

17 ⁶State Key Laboratory of Pollution Control and Resource Reuse and School of the Environment,
18 Nanjing University, Nanjing 210023, China

19
20 *Correspondence to:* Tianliang Zhao (tlzhao@nuist.edu.cn) and Kai Meng (macka@foxmail.com)

21 **Abstract:** The regional PM_{2.5} transport is one of the important causes for atmospheric
22 environment change. However, the variations of regional PM_{2.5} transport in synoptic scale with
23 meteorological drivers have been incomprehensively understood. Therefore, this study is targeted
24 at the quasi-weekly oscillation (QWO) of regional PM_{2.5} transport over central and eastern China
25 (CEC) with the influence of synoptic-scale disturbance of the East Asian Winter Monsoon
26 (EAWM) circulation. By constructing the data of daily PM_{2.5} transport flux in CEC in the winters
27 of 2015-2019, we utilize the extended empirical orthogonal function (EEOF) decomposition and
28 other statistical methods to extract the moving spatial distribution of regional PM_{2.5} transport over
29 CEC, recognizing the QWO in regional PM_{2.5} transport with the spatial-temporal variations over
30 CEC. The source-acceptor relationship in regional transport of PM_{2.5} is identified with the 2-d lag
31 effect of the North China Plain, as the upwind source region, on the PM_{2.5} pollution change in the
32 Twain-Hu Basin, as the downwind receptor region in central China. The QWO of regional PM_{2.5}
33 transport over CEC is regulated by the synoptic-scale disturbance of the EAWM circulation with
34 the periodic activities of Siberian high. These findings could provide new insight into the

35 understanding of regional $PM_{2.5}$ transport with source-receptor relationship and the meteorological
36 mechanism in atmospheric environment change.

37

38 **Key words:** regional $PM_{2.5}$ transport, quasi-weekly oscillation, source-receptor relationship,
39 extended empirical orthogonal function (EEOF)

40

41 **1 Introduction**

42 $PM_{2.5}$ pollution has attracted worldwide attention due to its adverse impact on the
43 environment and human health (Fan et al., 2016; Geng et al., 2021; Lin et al., 2018). The $PM_{2.5}$
44 pollution in the cold season has become one of the major atmospheric environmental problems in
45 China (An et al, 2019; Huang et al, 2020b). The high-concentration $PM_{2.5}$ tends to occur with
46 extensive spatiotemporal coverage (Tao et al, 2016; Zhang et al, 2019), and synthetic
47 physical-chemical processes caused such heavy $PM_{2.5}$ pollution events (Ding et al, 2017; Quan et
48 al., 2020), including emissions (Liu et al, 2016; Zheng et al, 2018a), chemical formation (Huang et
49 al, 2014; Nie et al, 2014), atmospheric boundary layer processes (Huang et al, 2018; Zhong et al,
50 2019), localized circulation (Miao et al, 2015; Shu et al, 2021; Zheng et al, 2018b), as well as
51 weather and climate (Cai et al, 2017; Wu et al, 2016). The interactions among these physical and
52 chemical processes make it more challenging to comprehend the severe haze formation, which
53 serves as one of the major difficulties in forecasting and controlling atmospheric environment
54 change and heavy air pollution (Zhang et al., 2012; Zhang et al., 2019).

55 $PM_{2.5}$ is featured with complex spatiotemporal changes on multiscale (Georgoulias and
56 Kourtidis, 2012; Wu et al, 2021). $PM_{2.5}$ oscillates periodically at multi-time scales, and the
57 periodic oscillation of atmospheric circulation is the leading cause of the cyclical variations of
58 $PM_{2.5}$ (Chen et al, 2020; Dong et al, 2021; Fu et al, 2020; Perrone et al, 2018). To be specific, the
59 1-d periodic change or diurnal variation of near-surface $PM_{2.5}$ concentrations is mainly attributed
60 to the atmospheric boundary layer process and localized circulation (Miao et al, 2019); the
61 periodic change of around 7 days may be controlled by the fluctuation of the long-wave trough in
62 middle and high latitudes (Guo et al, 2014); the oscillating cycle of about 14 days is closely
63 related to the quasi-biweekly oscillation of the synoptic circulation (Gao et al, 2020; Zhao et al,
64 2019); and the 30-60-d intra-seasonal oscillation is mainly caused by the impact of monsoon

65 circulation change (Xu et al, 2014; Zhang et al, 2019). Comprehensively revealing the interaction
66 between PM_{2.5} and meteorology at different time scales is essential for solving air pollution
67 problems more effectively (B äumer and Vogel, 2007; Wang et al, 2020). Previous studies mainly
68 focused on the multiscale periodic variation of atmospheric pollutants in a certain region or local
69 area, have not yet found on the PM_{2.5} trans-regional and periodic oscillation in the large area of
70 central and eastern China (CEC).

71 East Asian Winter Monsoon (EAWM) is one of the most active atmospheric circulation
72 system in the cold season over the Northern Hemisphere (Ding et al, 2017; Wu and Wang, 2002),
73 which is also a critical leading factor for the variation of wintertime air pollution in CEC (Chin,
74 2012; Li et al, 2016). Being the major circulation system of EAWM, the Siberian High dominates
75 the cold seasons, acting as a particular driver of cold airflows, so having an important impact on
76 the wintertime atmospheric environment in CEC (An et al, 2019; Shen et al, 2021, 2022; Wu et al,
77 2016). The rapid southward advance of cold air with strong Siberian High can effectively drive the
78 regional transport of air pollutants with less accumulations across CEC, while the weak Siberian
79 High with the slow southward movement of cold air can particularly favorable for the transport of
80 air pollutants from the northern source regions to southern receptor region over CEC (Hou et al.,
81 2020; Zhang et al., 2016). When the position of Siberian High is more eastern than normal, the
82 transport of air pollutants from northern China to the south is weakened, and the aggravation of
83 pollution is enhanced in northern China (Jia et al., 2015). Regional pollutant transport driven by
84 the southward movement of a cold front with the Siberian High would exacerbate the air quality in
85 the corresponding receptor regions (Kang et al., 2019; Hu et al., 2021; Shen et al, 2022). The
86 characteristics of atmospheric circulation anomalies favoring heavy haze pollution in China have
87 changed in recent years, and the leading formation mechanism of severe haze has been shifting
88 from local accumulation to regional transport processes in eastern China (Yang et al, 2021b).
89 Therefore, studying the influence of EAWM circulation system on regional pollutant transport
90 over CEC is an important issue in atmospheric environment changes (Bai et al, 2021, 2022; Ge et
91 al, 2018; Merrill and Kim, 2004; Tan et al, 2021; Yang, et al, 2021a).

92 Previous studies have primarily focused on the relationship between atmospheric
93 intraseasonal oscillations in the mid-to-high latitudes of the Eurasian region and the persistent
94 PM_{2.5} pollution (An et al., 2022; Gao et al., 2020; Li et al., 2021; Liu et al., 2022; Wu et al., 2023;

95 Yang et al., 2024b). $PM_{2.5}$ concentration anomalies in North China exhibit significant lifetimes of
96 10–30 days, with anticyclonic anomalies and related meteorological conditions (e.g., surface air
97 temperature, boundary layer height) in Northeast Asia influencing local $PM_{2.5}$ accumulation and
98 hygroscopic growth (An et al., 2022; Yang et al., 2024b). These studies have investigated the
99 quasi-biweekly lifecycle of persistent $PM_{2.5}$ pollution events in North China through phase
100 synthesis methods (Gao et al., 2020; Wu et al., 2023; Yang et al., 2024b). However, there remains
101 a lack of systematic studies on the synoptic-scale oscillation of regional $PM_{2.5}$ transport.

102 The “harbor” effect on the eastern lee of the Tibetan Plateau’s large topography on the
103 westerlies is possibly an important factor influencing the regional distribution of $PM_{2.5}$ pollution
104 in CEC with weak horizontal winds and sinking motion in the lower troposphere, which
105 exacerbates the environmental impacts of local air pollutant emissions establishing a
106 "susceptibility zone" in this region (Xu et al., 2016; Zhu et al, 2018). Anticyclones and cyclones
107 alternatively affect the region on a time scale of 3-7 days, resulting in periodic air pollution in
108 cities (Guo et al., 2014). Thus, the weather system in the CEC is basically characterized by
109 periodic changes and the cold air in winter with EAWM oscillates in quasi-weekly periods (Wu
110 and Wang, 2002; Wu et al., 2016). However, the influence of the synoptic-scale disturbance of the
111 EAWM on regional $PM_{2.5}$ transport over CEC is not yet clear. Responding to this problem, this
112 study aims to reveal from a new perspective the quasi-weekly oscillation (QWO) of regional $PM_{2.5}$
113 transport over CEC affected by EAWM and its underlying mechanism with the synoptic-scale
114 oscillation of the EAWM circulation. This study could deepen the understanding of regional $PM_{2.5}$
115 transport, its source-receptor relationship and meteorological mechanism in the atmospheric
116 environment changes, and provide scientific evidence for air pollution forecast, early warning and
117 coordinated control.

118

119 **2 Data and methods**

120 2.1 Environmental and meteorological data

121

122 The daily dataset of $PM_{2.5}$ concentrations selected for this study was from China National
123 Environmental Monitoring Center (<http://datacenter.mee.gov.cn/>), including daily $PM_{2.5}$
124 concentrations from 1079 air quality monitoring stations in CEC during the winters

125 (December-February) of 2015-2019.

126 Meteorological data were selected out of the NCEP/NCAR global reanalysis daily data
127 (<https://psl.noaa.gov/data/gridded/tables/daily.html>) with a grid resolution of $2.5^{\circ} \times 2.5^{\circ}$ for the
128 large-scale circulation analysis. It is composed of the daily sea level pressure (SLP), air
129 temperature at 1000 hPa, and the U- and V-components of wind at 1000 hPa during the winters of
130 2015–2019.

131 In addition, the ERA5-land high-resolution reanalysis hourly dataset
132 (<https://cds.climate.copernicus.eu/cdsapp#!/dataset/reanalysis-era5-land?tab=form>) with spatial
133 resolution of $0.1^{\circ} \times 0.1^{\circ}$ was selected for the calculation of transport flux (TF) of $PM_{2.5}$ in CEC.
134 The U- and V-components of the 10-m wind over CEC were obtained at 00, 06, 12, and 18 UTC
135 daily during the winter (December-February) of 2015-2019. In order to match the resolution of
136 $PM_{2.5}$ daily data, the ERA5-Land high-resolution 10-m wind was processed into daily average
137 data.

138

139 2.2 $PM_{2.5}$ TF and its divergence

140

141 In order to quantitatively characterize the horizontal transport direction and intensity of $PM_{2.5}$
142 as well as convergence or divergence during regional $PM_{2.5}$ transport, we introduced the concepts
143 of $PM_{2.5}$ TF and divergence of $PM_{2.5}$ TF. Generally, there are two types of TF: horizontal and
144 vertical. This study only addresses the near-surface horizontal $PM_{2.5}$ TF. The horizontal $PM_{2.5}$ TF
145 is defined as the $PM_{2.5}$ mass passing through the unit area in unit time (unit: $\mu\text{g m}^{-2} \text{s}^{-1}$), expressed
146 as the product of wind vector and $PM_{2.5}$ concentration (Liu et al., 2019; Ma et al., 2021), and its
147 vector points to the same direction as the horizontal wind. The zonal component (F_u) and
148 meridional component (F_v) of $PM_{2.5}$ TF vector (TFV) and the magnitude (TFM) are calculated as
149 follows:

$$150 \quad F_u = C u \quad (1)$$

$$151 \quad F_v = C v \quad (2)$$

$$152 \quad TFV = F_u i + F_v j \quad (3)$$

$$153 \quad TFM = \sqrt{F_u^2 + F_v^2} \quad (4)$$

154 where C is the surface $PM_{2.5}$ concentration, u and v are the zonal and meridional components
155 of the 10-m wind speed, respectively.

156 Firstly, the U- and V-components of ERA5-Land high-resolution 10-m wind are interpolated
157 to 1079 stations of environmental measurements in CEC for calculations of near-surface PM_{2.5} TF
158 in this study. Then, the daily PM_{2.5} TF of the 1079 stations for the winters from 2015 to 2019 are
159 calculated according to the calculation by Formulas (1)–(4).

160 The divergence of PM_{2.5} TF can be an indicator for the PM_{2.5} budget. When positive
161 divergence occurs, the air pollutants were net outflow from the domain region, and vice versa
162 (Wang et al., 2021). The divergence of horizontal PM_{2.5} TF near the surface is calculated as
163 follows (Wang et al., 2021):

$$164 \quad D = \frac{\partial F_u}{\partial x} + \frac{\partial F_v}{\partial y} \quad (5)$$

165 where D is the horizontal PM_{2.5} TF divergence, unit: $\mu\text{g m}^{-3} \text{s}^{-1}$. If D is positive (negative), it
166 indicates divergence (convergence) of PM_{2.5} TF.

167 In the i and j grids, the expression of Formula (5) for the differential calculation with grid
168 spacing to be d is

$$169 \quad D = \frac{Fu_{i+1,j} - Fu_{i-1,j} + Fv_{i,j+1} - Fv_{i,j-1}}{2d} \quad (6)$$

170 When calculating the horizontal divergence of transport PM_{2.5} flux, it is necessary to
171 interpolate the station data of zonal and meridional components (F_u , F_v) of PM_{2.5} TFV to grid
172 spacing with 0.25 by 0.25 degree in longitude and latitude in CEC and then calculate the
173 divergence of PM_{2.5} TF at each grid point according to Formula (6).

174

175 2.3 Butterworth filter

176

177 Atmospheric motion encompasses a variety of temporal and spatial scales. The sequences of
178 meteorological variables often contain complex periodic components and exhibit multi-time-scale
179 variations, including daily, weekly, seasonal, and interannual variations. Numerous observations
180 have found QWO with periods of less than 10 days across various meteorological elements in the
181 EAWM system (Compo et al., 1999; Murakami, 1979; Wu and Wang, 2002). Synoptic-scale
182 atmospheric variations are closely related to atmospheric longwave adjustments, with QWO
183 periods of 4-7 days observed in cold air activities of the EAWM (Bai et al., 2022; Wu and Wang,
184 2002). The synoptic-scale disturbance regulates the generation, transport, and removal of PM_{2.5} in
185 air pollution, which is a key mechanism behind the 4-7 day periodic changes in PM_{2.5} in CEC

186 during the periods of EAWM (Guo et al., 2014; Liu et al., 2018; Quan et al., 2014, 2020). Based
187 on the research objectives, identifying the desired periodic components from the original
188 observational sequences is referred to as sequence filtering. In this study, we employed a
189 Butterworth filter to extract QWO from observational data.

190 The Butterworth filter is commonly used to separate atmospheric periodic variations across
191 specific frequency bands. Due to its smooth amplitude response, linear phase characteristics, and
192 ease of implementation, Butterworth filter has been widely applied in climate and meteorological
193 studies (Gouirand et al., 2012; Yang et al., 2024a). The Butterworth filter can be configured as a
194 low-pass, high-pass, or band-pass filter, depending on the specific requirements. A band-pass
195 filtering only allows signals within a defined frequency range to pass through with attenuating
196 signals outside the defined frequency range. It is often employed to extract and analyze signals
197 within specific frequency bands, such as particular weather patterns and climate cycles. In this
198 study, to investigate the QWO (8-d) of regional PM_{2.5} transport over the CEC under the influence
199 of EAWM circulations in the synoptic scale, we applied Butterworth band-pass filtering to the
200 daily TFM of PM_{2.5} change and daily SLP anomalies during the winters of 2015-2019 for
201 identifying at the quasi-weekly (6-9 days) synoptic-scale component of regional transport of
202 PM_{2.5} over CEC.

203

204 2.4 Extended empirical orthogonal function (EEOF)

205

206 The Empirical Orthogonal Function (EOF) analysis is a widely-applied climate statistical
207 method in atmospheric and oceanographic scientific studies (Kim et al., 2015; Li et al., 2019;
208 Schepanski et al., 2016), also used to investigate the variability of atmospheric aerosols at
209 different spatiotemporal scales (Bai et al., 2022; Feng et al., 2020). The mathematical process of
210 EOF analysis is to decompose the variable field $X_{m \times n}$, which consists of observations at n times at
211 m spatial points, into a linear combination of p spatial eigenvectors (modes) with corresponding
212 time-weighting coefficients:

$$213 \quad X_{m \times n} = V_{m \times p} T_{p \times n} \quad (7)$$

214

215 where V is the spatial eigenvector (load) and T represents the time coefficient. The main
216 information of variable field $X_{m \times n}$ is represented by several eigenvectors. Since the method has

217 been maturely applied, the detailed calculation steps of EOF decomposition are omitted here, and
 218 our focus is on how to construct the observation matrix.

219 Firstly, we decompose the daily PM_{2.5} TFM anomalies of 1079 stations in CEC during the
 220 winters of 2015-2019 by EOF method. Thus, the following observation matrix can be obtained:

$$221 \quad X = \begin{bmatrix} X_{11} & \cdots & X_{1n} \\ \vdots & & \\ X_{m1} & \cdots & X_{mn} \end{bmatrix} \quad (8)$$

222 where X represents the PM_{2.5} TFM anomalies, m represents the spatial points for 1079
 223 stations, and n represents the observation times of 450 days. Then, the variable field X is
 224 decomposed into the sum of the product of space and time functions according to Formula (7).

225 EOF decomposition of PM_{2.5} TFV anomalies can be performed by employing the complex
 226 matrix, hence the following observation matrix is constructed:

$$227 \quad X = \begin{bmatrix} U_{11} & \cdots & U_{1n} \\ \vdots & & \\ U_{m1} & \cdots & U_{mn} \\ V_{11} & \cdots & V_{1n} \\ \vdots & & \\ V_{m1} & \cdots & V_{mn} \end{bmatrix} \quad (9)$$

228 where X is the PM_{2.5} TFV anomalies, and u and v refer to the zonal and meridional
 229 components of TFV anomalies.

230 With EOF analysis we can get the spatial distribution structure, which is in a fixed time
 231 pattern of climate variables, but we cannot get a temporally moving spatial distribution structure.
 232 EEOF is an extension of the EOF to analyze the autocorrelations of the variable field over time.
 233 By selecting a lag time, the original observational matrix is expanded into multiple continuous
 234 time matrices, diagnosing the temporal changes in the spatial structure of variable fields. This
 235 method has widespread applications in the analysis and prediction of marine and atmospheric
 236 motions (Dey et al., 2018; Qian et al., 2019; Wang et al., 2019).

237 In this study, we utilized the EEOF analysis to reveal the evolution of PM_{2.5} TF to reveal the
 238 spatiotemporal variations of regional PM_{2.5} transport. On the basis of Formula (8), a new extension
 239 matrix of PM_{2.5} TFM is constructed. Due to the study on the synoptic scale, 5 lag times are

240 selected, and each lag time is 1 day in length. The constructed observation matrix is as follows:

$$X = \begin{bmatrix} X_{1,1} & \cdots & X_{1,n-5} \\ \vdots & & \\ X_{m,1} & \cdots & X_{m,n-5} \\ X_{1,2} & \cdots & X_{1,n-4} \\ \vdots & & \\ X_{m,2} & \cdots & X_{m,n-4} \\ X_{1,3} & \cdots & X_{1,n-3} \\ \vdots & & \\ X_{m,3} & \cdots & X_{m,n-3} \\ X_{1,4} & \cdots & X_{1,n-2} \\ \vdots & & \\ X_{m,4} & \cdots & X_{m,n-2} \\ X_{1,5} & \cdots & X_{1,n-1} \\ \vdots & & \\ X_{m,5} & \cdots & X_{m,n-1} \\ X_{1,6} & \cdots & X_{1,n} \\ \vdots & & \\ X_{m,6} & \cdots & X_{m,n} \end{bmatrix} \quad (10)$$

241

242 Seen from Formula (10), the new extended matrix is composed of $X_{6m,n-5}$, where X is the
 243 $PM_{2.5}$ TFM anomalies, m is the spatial points of observation station, and n is the observation times
 244 of 450 days. When EEOF decomposition is performed on $PM_{2.5}$ TFV, the complex matrix is still
 245 used for the extension, and the same lag scheme is adopted to construct a new extended matrix of
 246 $PM_{2.5}$ TFV based on Formula (9). After constructing the initial data matrix, the EEOF
 247 decomposition method is in line with the classical EOF decomposition method.

248 Additionally, existing studies have utilized wavelet analysis, power spectrum analysis, and
 249 band-pass filtering methods to extract intraseasonal oscillation sequences of regional $PM_{2.5}$
 250 concentrations (An et al., 2022; Gao et al., 2020; Li et al., 2021; Liu et al., 2022; Wu et al., 2023;
 251 Yang et al., 2024b). Such approaches may serve as alternative methods to EEOF analysis for
 252 establishing the quasi-weekly lifecycle of regional $PM_{2.5}$ transport.

253

254 3 Results and discussion

255

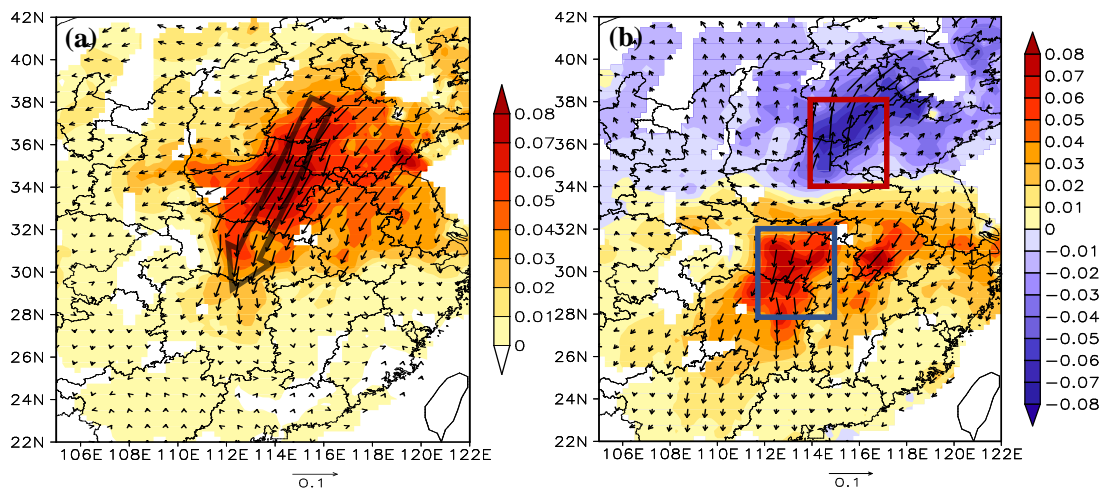
256 3.1 QWO of regional PM_{2.5} transport over CEC

257

258 The EOF decomposition is carried out on the daily anomalies of PM_{2.5} TFM and TFV in the
259 winters of 2015-2019 over CEC. The first two EOFs explain 26.6% and 14.2% (29.1% and 11.8%)
260 of the total anomalous variations of PM_{2.5} TFM (TFV), which is very helpful for better
261 characterizing regional PM_{2.5} transport variations.

262 Two principal modes govern the variations of PM_{2.5} TF anomalies over CEC: the first leading
263 mode of monopole (EOF1) and the second mode of meridional dipole (EOF2) (Fig. 1). EOF1
264 indicates the enhanced PM_{2.5} TF over CEC (Fig. 1a). The large value center of TF mainly occurs
265 in central China, and the transport vector direction is abnormally by north. The horizontal PM_{2.5}
266 transport is unusually strong in central China affected by the EAWM, presenting a typical channel
267 for regional PM_{2.5} transport over CEC (Yang et al., 2021a). The dipole mode of PM_{2.5} TF
268 anomalies displays a south–north out-of-phase pattern, with the flux large value centers located in
269 the North China Plain (NCP) and the Twain-Hu Basin (THB) respectively, and the vector
270 directions are opposite (Fig. 1b). This mode indicates that the air pollutants from NCP in the
271 upwind are transported to THB in the downwind driven by the prevailing northerlies of EAWM
272 (Hu et al., 2021; Shen et al., 2022), and the PM_{2.5} flux in NCP decreases while that in THB
273 increases in the regional PM_{2.5} transport process.

274



275

276 **Figure 1.** Spatial pattern of the (a) EOF1 and (b) EOF2 loads in the daily change of PM_{2.5} TFV anomalies (vectors,
277 unitless) and TFM anomalies (color contours, unitless) over CEC in the winters of 2015-2019. The red and blue
278 boxes indicate NCP and THB, respectively. The grid cells in white represent "missing values".

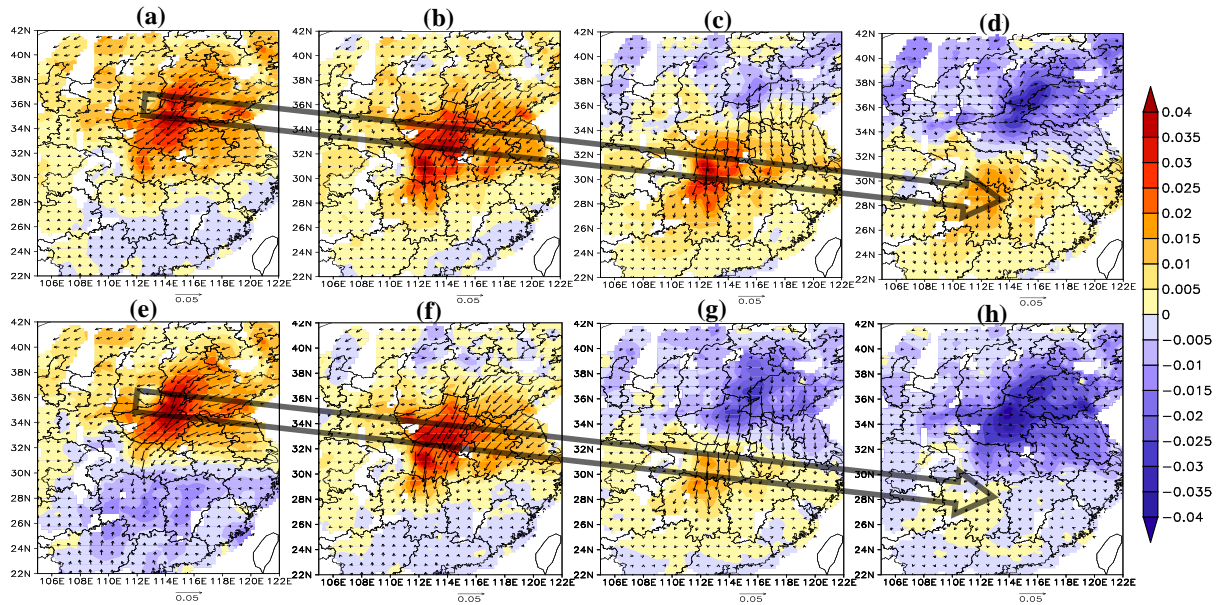
279

280 Through EOF decomposition, the $PM_{2.5}$ TF could be understood from the perspective of a
281 fixed time pattern of climate, but the temporal changes in the moving spatial structure of $PM_{2.5}$ TF
282 over CEC failed to be obtained. However, EEOF decomposition can be used to analyze the
283 continuous structural evolution of the main modes of regional $PM_{2.5}$ TF over CEC.

284 The EEOF decomposition was carried out for the daily variations of $PM_{2.5}$ TFM anomalies
285 and TFV anomalies respectively over CEC during the winters of 2015-2019. Figure 2 and Figure
286 S1 show the spatial distribution of different lag times for the main modes of EEOFs, which
287 account for about 20% of the total variation. According to the analysis, the $PM_{2.5}$ TFM anomalies
288 for EEOF2 and EEOF3, as well as TFV anomalies for EEOF1 and EEOF2, all show the structural
289 evolutions in the different phases of regional $PM_{2.5}$ transport in one cycle. As it can be seen,
290 Figures. 2a-d, S1a-d, and 2e-h respectively describe the evolution of the first and second four
291 phases in a cycle and the first four phases in the next cycle (one phase represents 1day).

292 Figures 2a-d illustrate the positive anomalies of $PM_{2.5}$ TF shifting from NCP to THB in the
293 first four phases under the effect of the EAWM, causing the upwind $PM_{2.5}$ TF to decrease and the
294 downwind $PM_{2.5}$ TF to increase, which is in line with the spatial pattern of the EOF modes in
295 Figure 1. The last four phases show the out-of-phase pattern of the first half cycle (Figs. S1a-d). It
296 is noted that when anomalies of $PM_{2.5}$ TFV in the NCP turn to the northerly direction (Fig. S1d
297 and Fig. 2e), it is a strong signal initiating the regional $PM_{2.5}$ transport. Then, the transport is
298 repeated in the next periodic cycle (Figs. 2e-h). Therefore, the regional $PM_{2.5}$ transport over CEC
299 enjoys a quasi-weekly (8-d) oscillation pattern.

300



301

302 **Figure 2.** (a)-(d) The first four phases (days) of QWO (8-d) during the regional PM_{2.5} transport over CEC; (e)-(h)
 303 the first four phases (days) of the next cycle. The Loads of PM_{2.5} TFM anomalies (color contours, unitless) for
 304 EEOF2 and TFV anomalies (vectors, unitless) for EEOF1 with lag time (a) 0 d, (b) 1 d, (c) 2 d and (d) 3 d, and
 305 loads of TFM anomalies (color contours, unitless) for EEOF3 and TFV anomalies (vectors, unitless) for EEOF2
 306 with lag time (e) 2 d, (f) 3 d, (j) 4 d and (h) 5 d over CEC in the winters of 2015-2019.

307

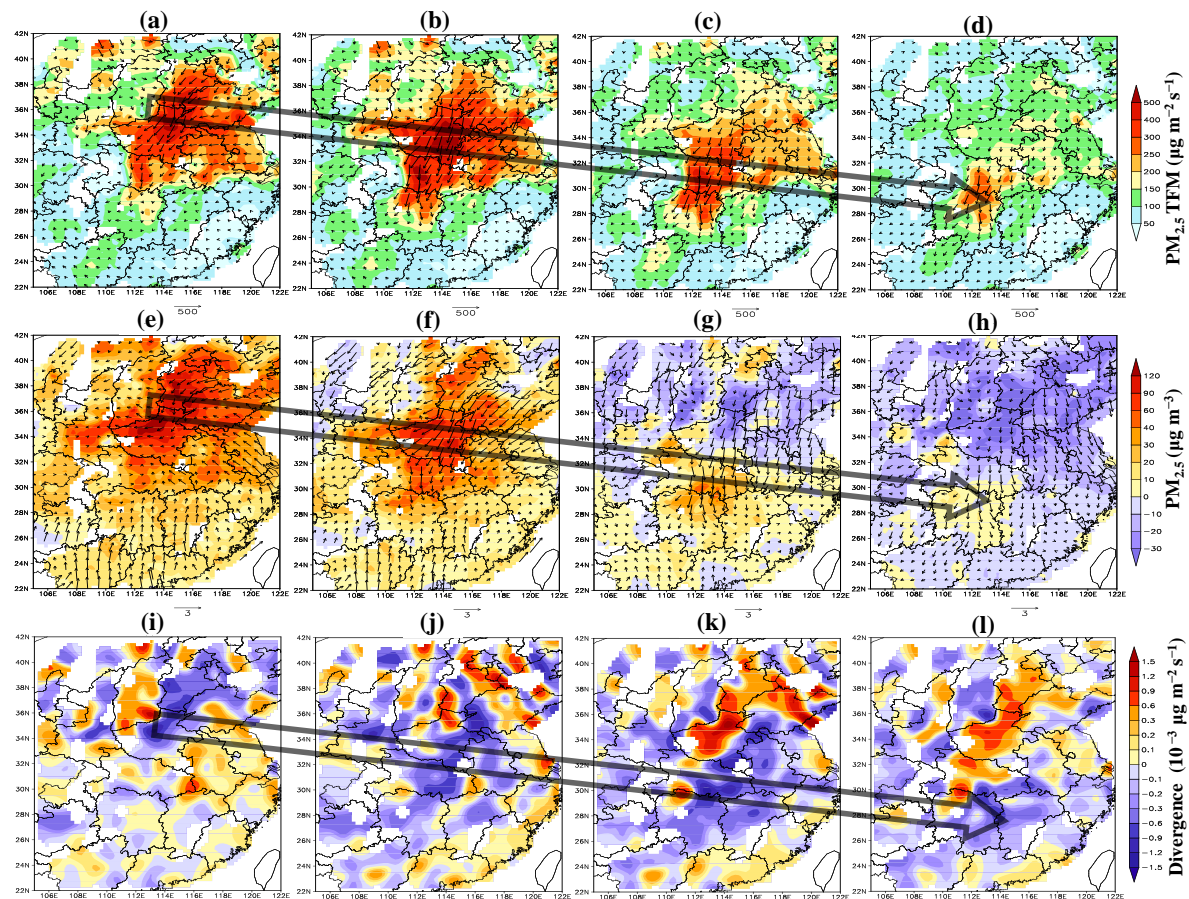
308 To further study the variations of regional PM_{2.5} transport over CEC, we have screened out
 309 23 typical events with greater than 1.5 times standard deviations based on the standardized time
 310 coefficient of EEOF, and then used the 8 consecutive days of each event as the 8 phases of QWO
 311 in the composite analysis on the 23 typical events of regional PM_{2.5} transport over CEC.

312 Figure 3 shows the composited PM_{2.5} TF, divergence of PM_{2.5} TF, and PM_{2.5} concentration
 313 anomalies in the first four phases of QWO. The high fluxes of PM_{2.5} transport from north to south
 314 persists for 3-4 days over CEC and decline in the THB (Fig. 3a-d). The regional PM_{2.5} transport
 315 lifetime corresponding to synoptic systems is about 3-5 days (Huang et al., 2020a). Abnormal
 316 northerly winds drive the heavy PM_{2.5} pollution from the upwind NCP to the downwind regions,
 317 aggravating PM_{2.5} pollution in the downwind THB (Figs. 3e-h). Under the context of QWO, the
 318 average PM_{2.5} TFM in NCP decreases from approximately 400 $\mu\text{g m}^{-2} \text{s}^{-1}$ in the 1st and 2nd phases
 319 to 200 and 100 $\mu\text{g m}^{-2} \text{s}^{-1}$ in the 3rd and 4th phases, respectively (Fig. S2a). Correspondingly, the
 320 PM_{2.5} concentration anomalies decline from around 100 $\mu\text{g m}^{-3}$ to approximately -50 $\mu\text{g m}^{-3}$ (Fig.
 321 S2c). In the downwind THB, the average PM_{2.5} TFM increases from about 200 $\mu\text{g m}^{-2} \text{s}^{-1}$ in the

322 1st phase to approximately $300 \mu\text{g m}^{-2} \text{s}^{-1}$ in the 2nd and 3rd phases (Fig. S2b), with $\text{PM}_{2.5}$
 323 concentration anomalies also rising to around $50 \mu\text{g m}^{-3}$ (Fig. S2d).

324 It is noteworthy that the regions $\text{PM}_{2.5}$ TF convergence zone (negative value of divergence)
 325 matches spatially the centers positive anomaly centers of $\text{PM}_{2.5}$ concentrations, which is confirmed
 326 with a significantly negative correlation of the $\text{PM}_{2.5}$ concentrations with divergences of $\text{PM}_{2.5}$ TF
 327 in the 23 typical events (Fig. S3). The $\text{PM}_{2.5}$ transport is accompanied by flux convergence, which
 328 is beneficial to the $\text{PM}_{2.5}$ accumulation. In addition, the $\text{PM}_{2.5}$ TF in the upwind NCP changes
 329 from convergence to divergence, and the divergence of the $\text{PM}_{2.5}$ TF in the downwind THB alters
 330 to convergence in the meantime (Figs. 3i-l), indicating that the $\text{PM}_{2.5}$ over THB is transported
 331 from the upwind NCP.

332



333

334 **Figure 3.** Spatial distributions of the composited (a-d) $\text{PM}_{2.5}$ TFM (color contours, unit: $\mu\text{g m}^{-2} \text{s}^{-1}$) and TFV
 335 (vectors, unit: $\mu\text{g m}^{-2} \text{s}^{-1}$), (e-h) anomalies of $\text{PM}_{2.5}$ concentrations (color contours, unit: $\mu\text{g m}^{-3}$) and 10-m wind
 336 vectors (unit: m s^{-1}), (i-l) divergence of $\text{PM}_{2.5}$ flux (color contours, unit: $10^{-3} \mu\text{g m}^{-3} \text{s}^{-1}$) in the first four phases of
 337 QWO during the 23 typical events of regional $\text{PM}_{2.5}$ transport over CEC.

338

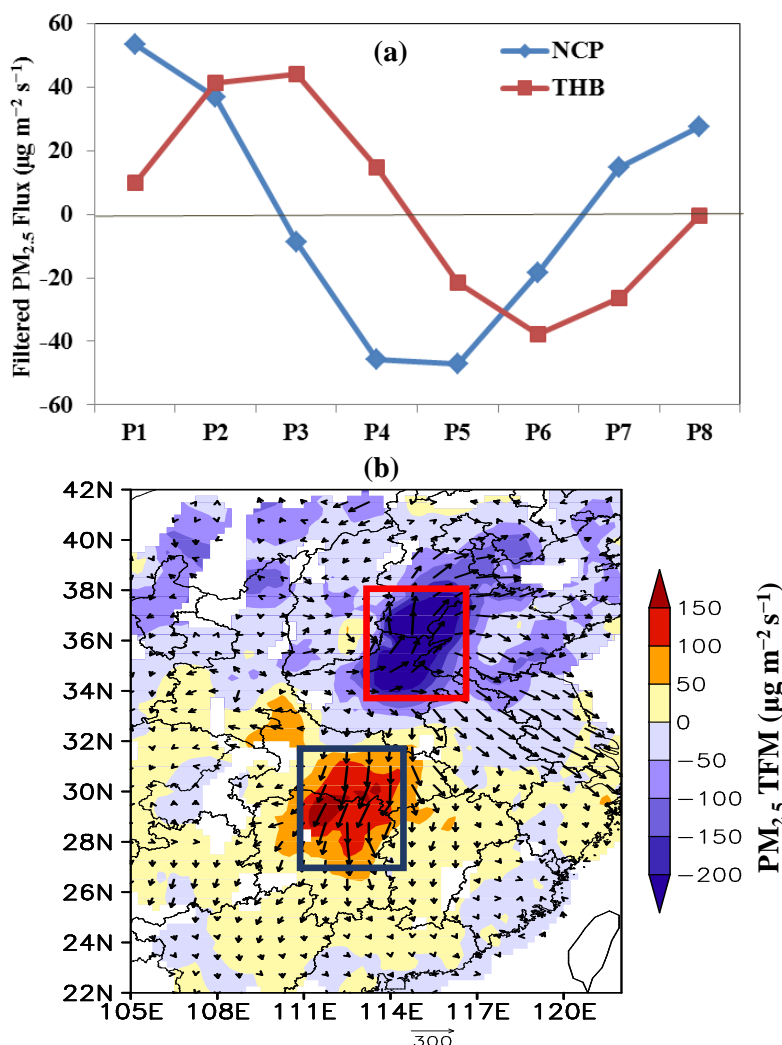
339 3.2 Source-receptor relationship in regional PM_{2.5} transport from NCP to THB

340

341 The regional pollutant transport governed by emissions and meteorology leads to a complex
342 source–receptor relationship of air pollution changes (Yu et al., 2020). Band-pass filtering is
343 performed on the daily PM_{2.5} TFM anomalies at a quasi-weekly (6-9 days) synoptic scale in the
344 winters of 2015-2019. In Figure 4a, we composite the filter components of PM_{2.5} TFM in the 8
345 phases of QWO during the 23 typical events of regional PM_{2.5} transport over the NCP and THB,
346 respectively. The PM_{2.5} TF exhibits an obvious QWO on the synoptic scale (Fig. 4a). The PM_{2.5}
347 TF over the NCP continues to decline in the first four phases, while that of THB first rises and
348 then falls in the last four phases, the PM_{2.5} TF over the NCP increases continuously, while that of
349 THB falls first and then rises. We can see that the QWO of PM_{2.5} TF over THB lags behind the
350 NCP by 2 phases (Fig. 4a). The high TFM of PM_{2.5} from NCP in the first phase spread to THB,
351 resulting in the peak of PM_{2.5} TF over THB in the third phase.

352 In addition, the distribution of the differences in PM_{2.5} TF and the vectors between phase 3
353 and phase 1 of the QWO, and the PM_{2.5} TF decrease and increase from phase 1 to phase 3
354 respectively over the upwind NCP and the downwind THB, which is in accordance with the
355 spatial pattern of the EOF mode (Figs.1b and 4b), indicating that the source-receptor relationship
356 over CEC exist the regions NCP and THB of regional PM_{2.5} transport over CEC.

357



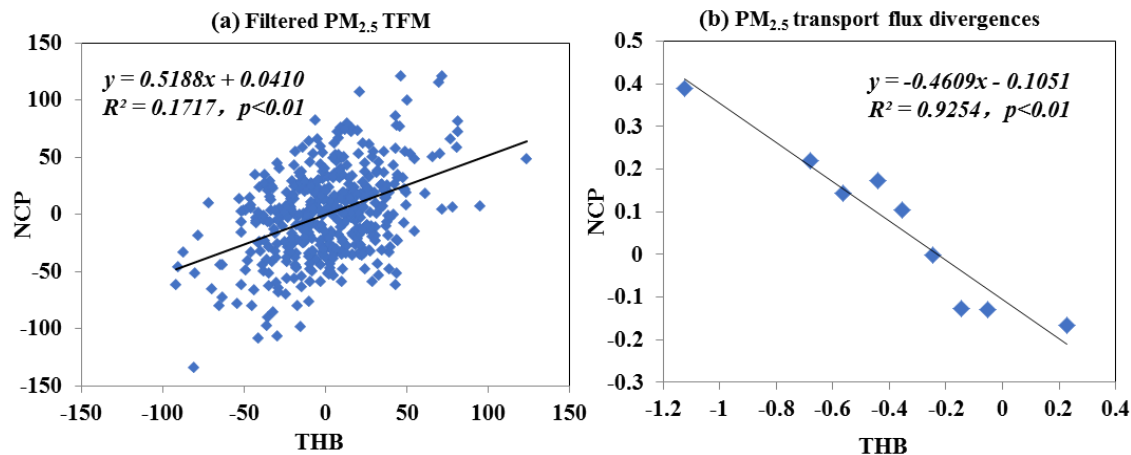
358

359 **Figure 4.** (a) The 8 phases (P1-P8) of QWO during the 23 typical events of regional $PM_{2.5}$ transport over the NCP
 360 and THB with composited 6-9 d band-pass filtering of $PM_{2.5}$ TFM; (b) spatial distribution of the differences in
 361 $PM_{2.5}$ TFM (color contours, unit: $\mu g m^{-2} s^{-1}$) and TFV (vectors, unit: $\mu g m^{-2} s^{-1}$) between the 3rd phase and the 1st
 362 phase of QWO. The red and black boxes represent NCP and THB.

363

364 The statistical analysis based on long-term observation also shows that there is a significant
 365 2-day lag relationship of positive correlation between NCP and THB in $PM_{2.5}$ TF in the QWO (Fig.
 366 5a). This discloses that the air pollutants are transported from the upwind NCP to the downwind
 367 THB in 2 days, confirming a quasi-2-d lag in the regional $PM_{2.5}$ transport from NCP to THB (Hu
 368 et al., 2021; Shen et al., 2021). Additionally, in the long-term change of air pollution, the
 369 divergences of $PM_{2.5}$ TF in the NCP are significantly negatively correlated to that of THB (Fig.
 370 5b), that is, the $PM_{2.5}$ TF convergences in the downwind THB fits well with the $PM_{2.5}$ TF

371 divergence in the upwind NCP. It can be reflected that the changes in the synoptic scale of EAWM
 372 atmospheric circulation impel the regional PM_{2.5} transport to build the source-receptor relationship
 373 of atmospheric pollutants between the NCP and THB.
 374



375
 376 **Figure 5.** (a) Scatter plot of 6-9-d filtering components of PM_{2.5} TFM ($10^{-3} \mu\text{g m}^{-2} \text{s}^{-1}$) over THB in 2-day lag and
 377 NCP during the winters of 2015-2019; (b) scatter plot of PM_{2.5} TF divergences ($10^{-3} \mu\text{g m}^{-3} \text{s}^{-1}$) between THB and
 378 NCP, and the PM_{2.5} TF divergences are averaged over the value interval of 0.1.

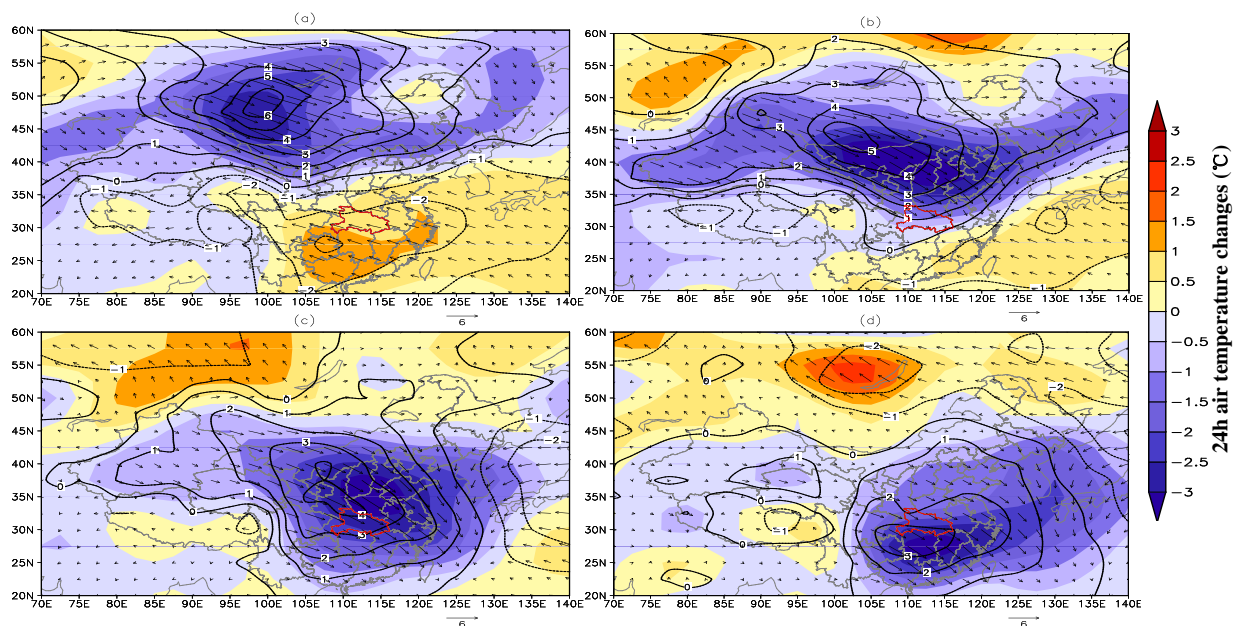
379
 380 Driven by prevailing winds of EAWM, the THB became the main receptor for regional
 381 transport of air pollutants over CEC (Bai et al., 2022; Shen et al., 2021). During 2015–2019,
 382 approximately 65.2% of the total PM_{2.5} heavy pollution events in the THB were triggered by
 383 regional transport of air pollutants over CEC (Hu et al., 2022; Shen et al., 2021). Such PM_{2.5}
 384 transport from upstream source regions in CEC contributes 51%-85.7% of the PM_{2.5} pollution
 385 over the THB receptor region (Hu et al., 2021; Lu et al., 2017; Shen et al., 2022; Yu et al., 2020),
 386 revealing the dominance of regional transport of air pollutants from CEC to the THB with the
 387 meteorological drivers. Our research emphasizes the QWO of regional PM_{2.5} transport over CEC
 388 with the driver of the synoptic-scale disturbances of EAWM circulation, confirming the
 389 source-receptor relationships with their 2-day lagging effects in the regional PM_{2.5} transport
 390 between the upstream NCP source region and the THB receptor region.

391
 392 3.3 Effect of synoptic-scale disturbance of EAWM circulation on QWO of regional PM_{2.5} transport
 393 over CEC

394
 395 Meteorological change is the essential factor in regulating the occurrence and development of

396 PM_{2.5} pollution on synoptic scales. To investigate the QWO of EAWM circulation in the synoptic
 397 scale disturbance, this study performs the 6-9-d band-pass filtering of the daily SLP anomalies
 398 (denoted as SLP_{QWO}) in East Asia during the winters of 2015-2019. The SLP and SLP_{QWO} fields
 399 (Figs. 6 and 7) as well as PM_{2.5} concentrations and 10-m winds (Fig. S4) in the 8 phases of QWO
 400 during the 23 typical events were composited, respectively. The QWO of regional PM_{2.5} transport
 401 is connected with the “weekly-cycle” synoptic process of PM_{2.5} transport and accumulation over
 402 CEC (Fig. S4), and it is powered mainly by the Siberian High circulation with the synoptic-scale
 403 disturbance of EAWM circulation (Figs. 6 and 7).

404



405

406 **Figure 6.** The composited differences between the current day and the previous day of SLP (black contour lines,
 407 unit: hPa), 1000 hPa air temperature (color contours, unit: °C) and wind vectors (unit: $m s^{-1}$) in the first four
 408 phases (a-d) of QWO during the 23 typical events.

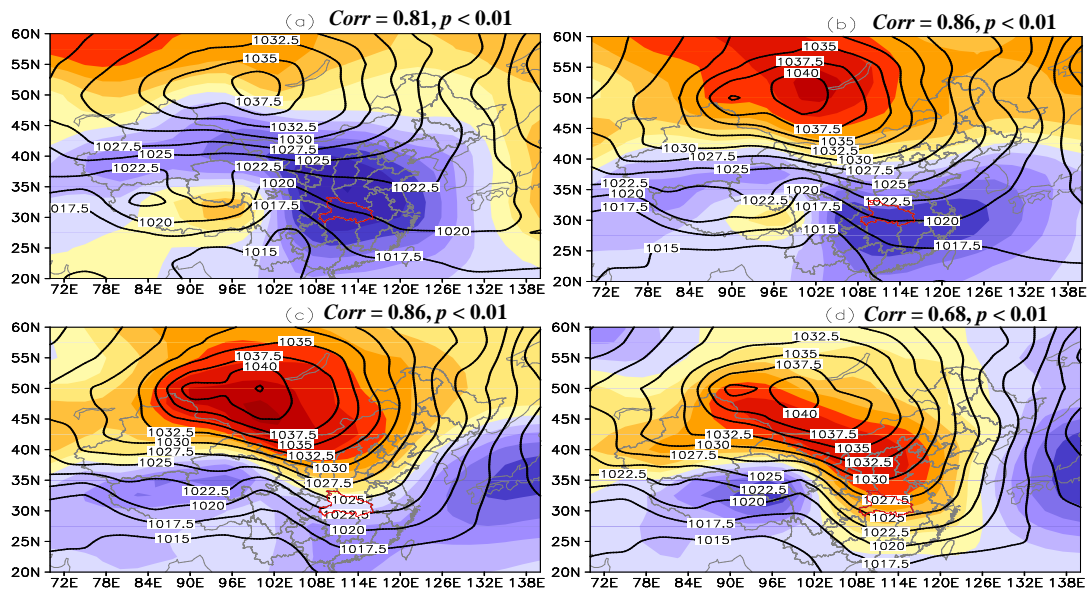
409

410 The condition of uniform pressure in the front of Siberian High could favor the PM_{2.5}
 411 accumulation over the NCP for triggering regional PM_{2.5} transport over CEC (Fig. 7a). The
 412 regional heavy pollution of PM_{2.5} >150 $\mu g m^{-3}$ lasts for 1-2 days (Figs. S4a and S4b). With the
 413 development of the Siberian High, the extension of the high pressure guides the cold air to
 414 advance southward (Park et al., 2014). As the result of the increasing air pressure gradients, the
 415 strong northerly winds in the EAWM circulation system, deliver high-level PM_{2.5} air mass from
 416 NCP to THB (Figs. 7a-d, Figs. S4a-d). In addition, the cold and high air pressure system with the

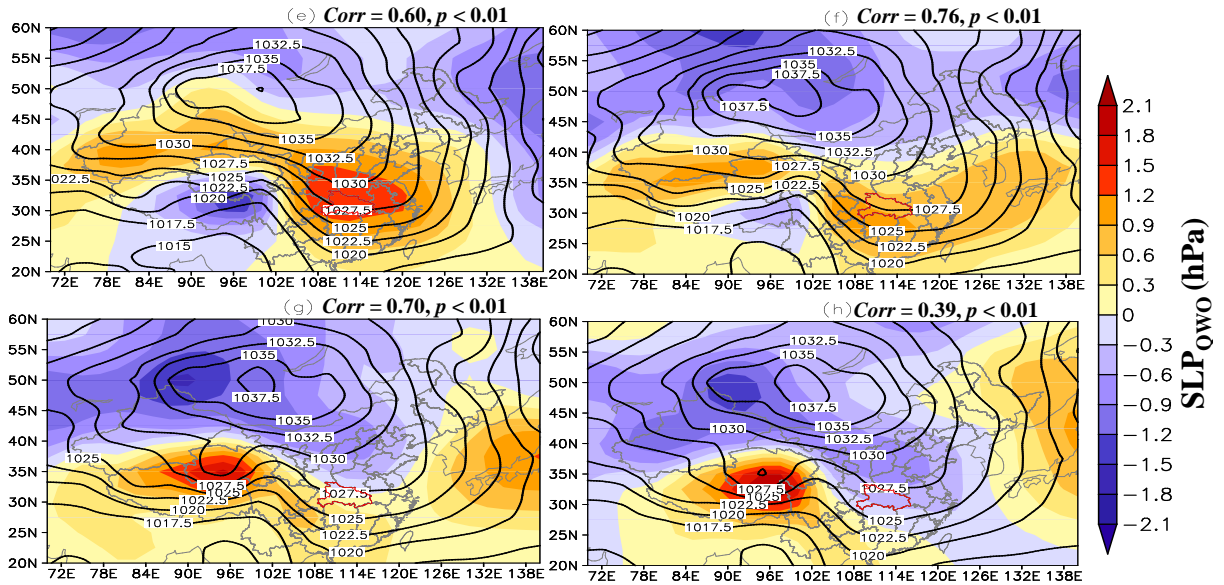
417 abnormal northerly airflows moves from the Siberia-Mongolia region to CEC in the first four
 418 phases (Fig. 6), providing beneficial synoptic circulation patterns for regional PM_{2.5} transport.
 419 Thus, the periodic extension of the Siberian High with the associated strong cold air intrusion is an
 420 important driver in the regional PM_{2.5} transport over CEC.

421 Notably, we can see that in the first four phases, the SLP_{QWO} positive anomalies occur,
 422 develop, and expand southward from the Siberia-Mongolia region to CEC (Figs. 7a-d). The
 423 synoptic-scale disturbance with the extension of Siberian High and the southward movement of
 424 cold air could drive the regional PM_{2.5} transport over CEC (Figs. 7a-d). The situation of the last
 425 four phases is opposite to the SLP_{QWO} negative anomalies in Siberia-Mongolia region, inhibiting
 426 the Siberian High and cold air intrusion (Figs. 7e-h). The low and uniform pressure is beneficial to
 427 the accumulation of PM_{2.5}. Therefore, the periodic changes in the synoptic-scale disturbance of the
 428 EAWM circulation impel the QWO of regional PM_{2.5} transport over CEC.

429



430



431

432 **Figure 7.** Composited SLP (black contour lines, unit: hPa) and its synoptic-scale filter component SLP_{QWO} (color
 433 contours, unit: hPa) in the 8 phases (a-h) of QWO during the 23 typical events. *Corr* represents the spatial
 434 correlation coefficients between SLP_{QWO} and the load of SLP_{QWO} decomposed by EEOF in Fig. S4.

435

436 In addition, the EEOF decomposition is carried out on the SLP_{QWO} field in the winters of
 437 2015-2019 to recognize the periodic activities in the synoptic scale of the EAWM circulation. The
 438 cold air activity of EAWM presents QWO (Wu and Wang, 2002). The positive (negative)
 439 synoptic-scale disturbance occurs in the Siberia-Mongolia region, and then spreads to CEC along
 440 the northwest-southeast path, contributing to the 8-d cycle of QWO (Fig. S5). Notably, the spatial
 441 correlation coefficients between the load of SLP_{QWO} decomposed by EEOF (Fig. S5) and the
 442 SLP_{QWO} composited during 23 typical events (Fig.7) are highly positively correlated in the 8
 443 phases, respectively. Therefore, the QWO in the synoptic-scale activities of the Siberian high is an
 444 important factor for driving the QWO of regional PM_{2.5} transport over CEC.

445

446 **4 Conclusions**

447 Exploring the periodical oscillations of PM_{2.5} pollution over CEC and the meteorological
 448 effect is crucial for understanding the change in the atmospheric environment and improving
 449 regional air quality forecasts. In this study with constructing a dataset of the daily PM_{2.5} TF, the
 450 EEOF and statistical methods are used to identify the QWO of regional PM_{2.5} transport with the
 451 spatiotemporal variations over CEC in winters from 2015 to 2019. The source-receptor

452 relationship is recognized between NCP and THB with the QWO of regional $PM_{2.5}$ transport over
453 CEC with the typical EAWM climate. Furthermore, it is revealed that the driving effect of
454 synoptic-scale disturbance of EAWM circulations on the QWO of regional $PM_{2.5}$ transport over
455 China.

456 The variations of $PM_{2.5}$ TF over CEC are dominated by the first leading monopole mode and
457 the second meridional dipole mode. The monopole mode indicates the high $PM_{2.5}$ flux along the
458 channel of regional $PM_{2.5}$ transport from NCP to THB under the governs of the EAWM
459 circulations, and the dipole mode exhibits a pattern of south-north out-phase with two centers
460 existing respectively in the upwind NCP and the downwind THB in regional transport of $PM_{2.5}$
461 over CEC. In terms of the long-term changes in air pollution of 2015–2019, the regional $PM_{2.5}$
462 transport over CEC is featured with the QWO, verifying a source-receptor relationship for the
463 regional $PM_{2.5}$ transport from NCP to THB in 2 days. Such changes are incurred by the QWO in
464 the activities of the Siberian High, and this synoptic-scale disturbance of the EAWM circulations
465 is generated in the Siberia-Mongolia region, and then develops, marching into CEC, regulating the
466 QWO of regional $PM_{2.5}$ transport.

467 The EEOF analysis with the temporal lag of the spatial fields is able to better characterize the
468 spatial and temporal evolution of perturbations, especially propagating waves in the atmosphere
469 (Weare and Nasstrom, 1982; Qian et al., 2019; Yang et al., 2024b). Due to its technical advantages,
470 the EEOF method is commonly employed to extract atmospheric oscillation patterns to reveal the
471 impacts and mechanisms of atmospheric fluctuations and monsoon circulation on regional weather,
472 climate, and atmospheric environments (Dey et al., 2018; Qian et al., 2019; Yang et al., 2024b). In
473 this study, we employed the EEOF method to identify regional $PM_{2.5}$ transport modes in synoptic
474 scale, by constructing $PM_{2.5}$ transport flux vectors (TFV) and the magnitude (TFM) with the
475 product of near-surface $PM_{2.5}$ concentrations and wind components at 1079 stations across China
476 during the winters of 2015-2019. We performed EEOF analysis on $PM_{2.5}$ TFV and TFM, resulting
477 in the spatial structure of $PM_{2.5}$ transport flux under the temporal disturbances at the synoptic scale,
478 and revealing the connection between synoptic-scale disturbances in the EAWM and QWO in
479 regional $PM_{2.5}$ transport in CEC. Our study focuses on the driving effects of synoptic-scale
480 disturbances associated with cold air activity with the anomalous northerly winds in EAWM on
481 QWO of regional $PM_{2.5}$ transport over CEC, exacerbating $PM_{2.5}$ pollution in the downwind THB.

482 Differently from the studies on stagnant meteorological conditions associated with PM_{2.5}
483 accumulations (Gao et al., 2020; Wu et al., 2023; Yang et al., 2024b), this study provides new
484 insights into the understanding of regional PM_{2.5} transport with source-receptor relationship with
485 the meteorological mechanism in atmospheric environment change.

486 Based on the 5-winter (2015-2019) observations of PM_{2.5} concentrations and the
487 corresponding meteorological reanalysis data, this study with the climate statistical and diagnostic
488 methods investigates the QWO of regional PM_{2.5} transport in China with the influence of
489 synoptic-scale disturbance of EAWM circulation, providing a new insight into the understanding
490 of regional air pollutant transport with meteorological drivers in atmospheric environment changes.
491 Besides the EEOF method used in this study, the alternative methods of wavelet analysis, power
492 spectrum analysis, and band-pass filtering could be used in further study. Future studies with
493 utilizing long-term observations of air pollutants and meteorology over CEC could more
494 comprehensively understand the variations in the regional transport of particles and the gaseous
495 precursors with their contributions to air pollution, through the integration of artificial intelligence
496 and physical-chemical process analyses.

497

498 *Data availability.* All data used in this paper can be provided upon request from Yongqing Bai
499 (2007byq@163.com)

500 *Author contributions.* YB and TZ conceived the study. YB designed the graphics and wrote the
501 manuscript with help from TZ, KM, YZ, JX, XS, LS, YY, YZ, WH and JY were involved in the
502 scientific discussion. All authors commented on the paper.

503 *Competing interests.* The authors declare that they have no conflict of interest.

504 *Financial support.* This research was supported by the National Natural Science Foundation of
505 China (grant no. 42075186, 41830965) and the National Key Research and Development Program
506 of China (2022YFC3701204).

507 **References**

508 An, X., Chen, W., Hu, P., Chen, S., and Zhang, Q.: Intraseasonal variation of the northeast Asian anomalous
509 anticyclone and its impacts on PM_{2.5} pollution in the North China Plain in early winter. *Atmos. Chem. Phys.*,

510 22, 6507–6521, <https://doi.org/10.5194/acp-22-6507-2022>, 2022.

511 An, Z., Huang, R., Zhang, R., Tie, X., Li, G., Cao, J., Zhou, W., Shi, Z., Han, Y., Gu, Z., and Ji, Y.: Severe haze in
512 northern China: A synergy of anthropogenic emissions and atmospheric processes. *P. Natl. Acad. Sci. USA*,
513 116, 8657–8666, <https://doi.org/10.1073/pnas.1900125116>, <https://doi.org/10.1073/pnas.1900125116>, 2019.

514 Bai, Y., Zhao, T., Zhou, Y., Kong, S., Hu, W., Xiong, J., Liu, L., Zheng, H., and Meng, K.: Aggravation effect of
515 regional transport on wintertime PM_{2.5} over the middle reaches of the Yangtze River under China’s air pollutant
516 emission reduction process. *Atmos. Pollut. Res.*, 12, 101111, <https://doi.org/10.1016/j.apr.2021.101111>, 2021.

517 Bai, Y., Zhao, T., Hu, W., Zhou, Y., Xiong, J., Wang, Y., Liu, L., Shen, L., Kong, S., Meng, K., and Zheng, H.:
518 Meteorological mechanism of regional PM_{2.5} transport building a receptor region for heavy air pollution over
519 Central China. *Sci. Total Environ.*, 808, 151951, <https://doi.org/10.1016/j.scitotenv.2021.151951>, 2022.

520 B äumer, D., and Vogel, B.: An unexpected pattern of distinct weekly periodicities in climatological variables in
521 Germany. *Geophys. Res. Lett.*, 34, L03819, <https://doi.org/10.1029/2006gl028559>, 2007.

522 Cai, W., Li, K., Liao, H., Wang, H., and Wu, L.: Weather conditions conducive to Beijing severe haze more
523 frequent under climate change. *Nat. Clim. Chang.*, 7, 257–262, <https://doi.org/10.1038/nclimate3249>, 2017.

524 Chen, X., Yin, L., Fan Y., Song, L., Ji, T., Liu, Y., Tian, J., and Zheng, W.: Temporal evolution characteristics of
525 PM_{2.5} concentration based on continuous wavelet transform, *Sci. Total Environ.*, 699,
526 <https://doi.org/10.1016/j.scitotenv.2019.134244>, 2020.

527 Chin M.: Dirtier air from a weaker monsoon. *Nat. Geosci.*, 5, 449–450, <https://doi.org/10.1038/ngeo1513>, 2012.

528 Compo, G. P., Kiladis, G. N. and Webster, P. J.: The horizontal and vertical structure of east Asian winter monsoon
529 pressure surges. *Quart. J. Roy. Meteor. Soc.*, 125, 29–54, <https://doi.org/10.1256/smsqj.55302>, 1999.

530 Dey, A., Chattopadhyay, R., Sahai, A. K., Mandal, R., Joseph, S., Phani, R., and Abhilash, S.: An operational
531 tracking method for the MJO using extended empirical orthogonal functions, *Pure. Appl. Geophys.*, 176, 2697–
532 2717, <https://doi.org/10.1007/s00024-018-2066-8>, 2018.

533 Ding, A., Huang, X., and Fu, C.: Air Pollution and Weather Interaction in East Asia, Oxford Research
534 Encyclopedia-Environmental Science, <https://doi.org/10.1093/acrefore/9780199389414.013.536>, 2017.

535 Dong, Y., Zhou, H., Fu, Y., Li, X., and Geng, H.: Wavelet periodic and compositional characteristics of
536 atmospheric PM_{2.5} in a typical air pollution event at Jinzhong city, China, *Atmos. Pollut. Res.*, 12, 245–254,
537 <https://doi.org/10.1016/j.apr.2020.09.013>, 2021.

538 Fan, J., Wang, Y., Rosenfeld, D., and Liu, X.: Review of aerosol–cloud interactions: Mechanisms, significance, and
539 challenges. *J. Atmos. Sci.*, 73, 4221–4252, <https://doi.org/10.1175/jas-d-16-0037.1>, 2016.

540 Feng, J., Zhu, J., Li, J., and Liao, H.: Aerosol concentrations variability over China: two distinct leading modes.
541 *Atmos. Chem. Phys.*, 20, 9883–9893, <https://doi.org/10.5194/acp-20-9883-2020>, 2020.

542 Fu, H., Zhang, Y., Liao C., Mao, L., Wang, Z., and Hong, N.: Investigating PM_{2.5} responses to other air pollutants
543 and meteorological factors across multiple temporal scales, *Sci. Rep.*, 10, 15639,
544 <https://doi.org/10.1038/s41598-020-72722-z>, 2020.

545 Gao, L., Wang, T., Ren X., Zhuang, B., Li, Shu., Yao, R., and Yang, X.: Impact of atmospheric quasi-biweekly
546 oscillation on the persistent heavy PM_{2.5} pollution over Beijing-Tianjin-Hebei region, China during winter,
547 *Atmos. Res.*, 242, 105017, <https://doi.org/10.5194/egusphere-egu2020-1398>, 2020.

548 Ge, B., Wang, Z., Lin, W., Xu, X., Li, J., Ji, D., and Ma, Z.: Air pollution over the North China Plain and its
549 implication of regional transport: A new sight from the observed evidences, *Environ. Pollut.*, 234, 29–38,
550 <https://doi.org/10.1016/j.envpol.2017.10.084>, 2018.

551 Geng, G., Zheng, Y., Zhang Q., Xue, T., Zhao, H., Tong, D., Zheng, B., Li, M., Liu, F., Hong, C., He, K., and
552 Davis, S. J.: Drivers of PM_{2.5} air pollution deaths in China 2002–2017, *Nat. Geosci.*, 14, 645–650,
553 <https://doi.org/10.1038/s41561-021-00792-3>, 2021.

554 Georgoulias, A. K., and Kourtidis, K. A.: A high resolution satellite view of the aerosol weekly cycle variability
555 over Central Europe. *Atmos. Res.*, 107, 145–160, <https://doi.org/10.1016/j.atmosres.2012.01.003>, 2012.

556 Gouirand, I., Jury, M. R., and Sing, B.: An analysis of low- and high-frequency summer climate variability around
557 the Caribbean Antilles. *J. Climate*, 25, 3942–3952, <https://doi.org/10.1175/jcli-d-11-00269.1>, 2012.

558 Guo, S., Hu, M., Zamora, M. L., Peng, J., and Zhang, R.: Elucidating severe urban haze formation in China. *P. Natl.*
559 *Acad. Sci. USA*, 111, 17373–17378, <https://doi.org/10.1073/pnas.1419604111>, 2014.

560 Hou, X., Zhu, B., Kumar, K. R., de Leeuw, G., Lu, W., Huang, Q., and Zhu, X.: Establishment of conceptual
561 schemas of surface synoptic meteorological situations affecting fine particulate pollution across eastern China
562 in the winter. *J. Geophys. Res.-Atmos.*, 125, e2020JD033153, <https://doi.org/10.1029/2020jd033153>, 2020.

563 Hu, W., Zhao, T., Bai, Y., Kong, S., Xiong, J., Sun, X., Yang, Q., Gu, Y., and Lu, H.: Importance of regional PM_{2.5}
564 transport and precipitation washout in heavy air pollution in the Twain-Hu Basin over Central China:
565 Observational analysis and WRF-Chem simulation. *Sci. Total Environ.*, 758, 143710,
566 <https://doi.org/10.1016/j.scitotenv.2020.143710>, 2021.

567 Hu, W., Zhao, T., Bai, Y., Kong, S., Shen, L., Xiong, J., Zhou, Y., Gu, Y., Shi, J., Zheng, H., Sun, X., and Meng, K.:
568 Regulation of synoptic circulation in regional PM_{2.5} transport for heavy air pollution: Study of 5-year
569 observation over central China. *J. Geophys. Res.-Atmos.*, 127, e2021JD035937,
570 <https://doi.org/10.1029/2021JD035937>, 2022.

571 Huang, R. J., Zhang, Y., Bozzetti, C., Ho, K. F., Cao, J. J., Han, Y., Daellenbach, K. R., Slowik, J. G., Platt, S. M.,
572 Canonaco, F., Zotter, P., Wolf, R., Pieber, S. M., Bruns, E., A., Crippa, M., Ciarelli, G., Piazzalunga, A.,
573 Schwikowski, M., Abbaszade, G., Kreis, J. S., Zimmermann, R., An, Z., Szidat, S., Baltensperger, U., Haddad,
574 I. E., and Prevot, A. S. H.: High secondary aerosol contribution to particulate pollution during haze events in
575 China. *Nature*, 514, 218–222, <https://doi.org/10.1038/nature13774>, 2014.

576 Huang, X., Wang, Z., and Ding, A.: Impact of aerosol-PBL interaction on haze pollution: Multiyear observational
577 evidences in North China. *Geophys. Res. Lett.*, 45, 8596–8603, <https://doi.org/10.1029/2018gl079239>, 2018.

578 Huang, H., Wang, S., Huang, W., Lin, N., Chuang, M., Silva, A. M., and Peng, C.: Influence of synoptic-dynamic
579 meteorology on the long-range transport of Indochin biomass burning aerosols. *J. Geophys. Res.-Atmos.*, 125,
580 e2019JD031260, <https://doi.org/10.1029/2019jd031260>, 2020a.

581 Huang, X., Ding, A., Wang, Z., Ding, K., Gao, J., Chai, F., and Fu, C.: Amplified transboundary transport of haze
582 by aerosol–boundary layer interaction in china. *Nat. Geosci.*, 13, 428–434,
583 <https://doi.org/10.1038/s41561-020-0583-4>, 2020b.

584 Jia, B., Wang, Y., Yao, Y., and Xie, Y.: A new indicator on the impact of large-scale circulation on wintertime
585 particulate matter pollution over China. *Atmos. Chem. Phys.*, 15, 11919–11929,
586 <https://doi.org/10.5194/acp-15-11919-2015>, 2015.

587 Kang, H., Zhu, B., Gao, J., He, Y., Wang, H., Su, J., Pan, C., Zhu, T., and Yu, B.: Potential impacts of cold frontal
588 passage on air quality over the Yangtze River Delta, China. *Atmos. Chem. Phys.*, 19, 3673–3685,
589 <https://doi.org/10.5194/acp-19-3673-2019>, 2019.

590 Kim, B. H., and Ha, K. J.: Observed changes of global and western Pacific precipitation associated with global
591 warming SST mode and mega-ENSO SST mode. *Clim. Dynam.*, 45, 3067–3075,
592 <https://doi.org/10.1007/s00382-015-2524-2>, 2015.

593 Li, Q., Zhang, R., and Wang, Y.: Interannual variation of the wintertime fog-haze days across central and eastern
594 China and its relation with EAWM. *Int. J. Climatol.*, 36, 346–354, <https://doi.org/10.1002/joc.4350>, 2016.

595 Li, X., Gereon, G., Greatbatch, R. J., and Lu, R.: Impact of the MJO on the interannual variation of the Pacific–
596 Japan mode of the East Asian summer monsoon. *Clim. Dynam.*, 52, 3489–3501,
597 <https://doi.org/10.1007/s00382-018-4328-7>, 2019.

598 Li, X., Yu, C., Deng, X., He, D., Zhao, Z., Mo, H., Mo, J., and Wu, Y.: Mechanism for synoptic and intra-seasonal
599 oscillation of visibility in Beijing-Tianjin-Hebei region. *Theor. Appl. Climatol.*, 143, 1005–1015,
600 <https://doi.org/10.1007/s00704-020-03466-z>, 2021.

601 Lin, Y., Zou, J., Yang, W., and Li, C. Q.: A Review of Recent Advances in Research on PM_{2.5} in China, *Int. J.*,
602 *Env., Res., Pub., He.*, 15, 438, <https://doi.org/10.3390/ijerph15030438>, 2018.

603 Liu, J., Huang, W., and Zhang, Q.: The quasi-biweekly oscillation of eastern China PM_{2.5} in response to different
604 Rossby wave trains over the Eurasian continent. *Atmos. Res.*, 267, 105990,
605 <https://doi.org/10.1016/j.atmosres.2021.105990>, 2022.

606 Liu, J., Mauzerall, D. L., Chen, Q., Zhang, Q., Song, Y, Peng, W., Klimont, Z., Qiu, X., Zhang, S., Hu, M., Lin, W.,
607 Smith, K. R., and Zhu, T.: Air pollutant emissions from Chinese households: A major and underappreciated
608 ambient pollution sources. *P. Natl. Acad. Sci. USA*, 113, 7756–7761, <https://doi.org/10.1073/pnas.1604537113>,
609 2016.

610 Liu, Q., Jia, X., Quan, J., Li, J., Li, X., Wu, Y., Chen, D., Wang, Z., and Liu, Y.: New positive feedback mechanism
611 between boundary layer meteorology and secondary aerosol formation during severe haze events. *Sci. Rep.*, 8,
612 6095, <https://doi.org/10.1038/s41598-018-24366-3>, 2018.

613 Liu, Y., Tang, G., Zhou, L., Hu, B., Liu, B., Li, Y., Liu, S., and Wang, Y.: Mixing layer transport flux of particulate
614 matter in Beijing, China. *Atmos. Chem. Phys.*, 19, 9531–9540, <https://doi.org/10.5194/acp-19-9531-2019>,
615 2019.

616 Lu, M., Tang, X., Wang, Z., Gbaguidi, A., Liang, S., Hu, K., Wu, L., Wu, H., Huang, Z., and Shen, L.: Source
617 tagging modeling study of heavy haze episodes under complex regional transport processes over Wuhan
618 megacity, Central China. *Environ. Pollut.*, 231, 612–621, <https://doi.org/10.1016/j.envpol.2017.08.046>, 2017.

619 Ma, Y., Zhu, Y., Liu, B., Li, H., Jin, S., Zhang, Y., Fan, R., and Gong, W.: Estimation of the vertical distribution of
620 particle matter (PM_{2.5}) concentration and its transport flux from lidar measurements based on machine learning
621 algorithms. *Atmos. Chem. Phys.*, 21, 17003–17016, <https://doi.org/10.5194/acp-21-17003-2021>, 2021.

622 Merrill, J. T., and Kim, J.: Meteorological events and transport patterns in ACE-Asia. *J. Geophys. Res.-Atmos.*,
623 109, D19S18, <https://doi.org/10.1029/2003jd004124>, 2004.

624 Miao, Y., Hu, X.M., Liu, S., Qian, T., Xue, M., Zheng, Y., and Wang, S.: Seasonal variation of local atmospheric
625 circulations and boundary layer structure in the Beijing-Tianjin-Hebei region and implications for air quality. *J.*
626 *Adv. Model. Earth Sys.*, 7, 1602–1626, 2015.

627 Miao, Y., Li, J., Miao, S., Che, H., Wang, Y., Zhang, X., Zhu, R., and Liu, S.: Interaction between planetary
628 boundary layer and PM_{2.5} pollution in megacities in China: a review. *Curr. Pollut. Rep.*, 5, 261–271,
629 <https://doi.org/10.1002/2015ms000522>, 2019.

630 Murakami, T.: Winter monsoonal surges over East and Southeast Asia. *J. Meteor. Soc. Japan.*, 57, 133–158,
631 https://doi.org/10.2151/jmsj1965.57.2_133, 1979.

632 Nie, W., Ding, A., Wang, T., Kerminen, V. M., George, C., Xue, L., Wang, W., Zhang, Q., Petäjä T., Qi, X., Gao,
633 X., Wang, X., Yang, X., Fu, C., and Kulmala, M.: Polluted dust promotes new particle formation and growth.
634 *Sci. Rep.*, 4, 6634, <https://doi.org/10.1038/srep06634>, 2014.

635 Park, T. W., Ho, C. H. and Deng, Y.: A synoptic and dynamical characterization of wave-train and blocking cold
636 surge over East Asia, *Clim. Dynam.*, 43, 753–770, <https://doi.org/10.1007/s00382-013-1817-6>, 2014.

637 Perrone, M. R., Vecchi, R., Romano, S., Becagli, S., Traversi, R., and Paladini, F.: Weekly cycle assessment of PM
638 mass concentrations and sources, and impacts on temperature and wind speed in Southern Italy. *Atmos. Res.*,
639 218, 129–144, <https://doi.org/10.1016/j.atmosres.2018.11.013>, 2018.

640 Qian, Y., Hsu, P. C., and Kazuyoshi, K.: New real-time indices for the quasi-biweekly oscillation over the Asian
641 summer monsoon region. *Clim. Dynam.*, 53, 2603–2624, <https://doi.org/10.1007/s00382-019-04644-0>, 2019.

642 Quan, J., Tie, X., Zhang, Q., Liu, Q., Li, X., Gao, Y., and Zhao, D.: Characteristics of heavy aerosol pollution
643 during the 2012–2013 winter in Beijing, China. *Atmos. Environ.*, 88, 83–89.
644 <https://doi.org/10.1016/j.atmosenv.2014.01.058>, 2014.

645 Quan, J., Xu, X., Jia, X., Liu, S., Miao, S., Xin, J., Hu, F., Wang, Z., Fan, S., Zhang, H., Mu, Y., Dou, Y., and
646 Cheng, Z.: Multi-scale processes in severe haze events in China and their interactions with aerosols:
647 Mechanisms and progresses. *Chin. Sci. Bull.*, 65, 810–824, <https://doi.org/10.1360/tb-2019-0197>, 2020.

648 Schepanski, K., Mallet, M., Heinold, B., and Ulrich, M.: North African dust transport toward the western
649 Mediterranean basin: Atmospheric controls on dust source activation and transport pathways during
650 June–July 2013. *Atmos. Chem. Phys.*, 16, 14147–14168, <https://doi.org/10.5194/acp-16-14147-2016>, 2016.

651 Shen, L., Hu, W., Zhao, T., Bai, Y., Wang, H., Kong, S., and Zhu, Y.: Changes in the Distribution Pattern of PM_{2.5}
652 Pollution over Central China. *Remote Sens.*, 13, 4855, <https://doi.org/10.3390/rs13234855>, 2021.

653 Shen, L., Zhao, T., Liu, J., Wang, H., Bai, Y., Kong, S., and Shu, Z.: Regional transport patterns for heavy PM_{2.5}
654 pollution driven by strong cold airflows in Twain-Hu Basin, Central China. *Atmos. Environ.*, 269, 118847,
655 <https://doi.org/10.1016/j.atmosenv.2021.118847>, 2022.

656 Shu, Z., Liu, Y., Zhao, T., Xia, J., Wang, C., Cao, L., Wang, H., Zhang, L., Zheng, Y., Shen, L., Luo, L., and Li, Y.:
657 Elevated 3D structures of PM_{2.5} and impact of complex terrain-forcing circulations on heavy haze pollution
658 over Sichuan Basin, China. *Atmos. Chem. Phys.*, 21, 9253–9268, <https://doi.org/10.5194/acp-21-9253-2021>,
659 2021.

660 Tan, Q., Ge, B., Xu, X., Gan, L., Yang, W., Chen, X., Pan, X., Wang, W., Li, J., and Wang, Z.: Increasing impacts
661 of the relative contributions of regional transport on air pollution in Beijing: Observational evidence, *Environ.*
662 *Pollut.*, 292, 118407, <https://doi.org/10.1016/j.envpol.2021.118407>, 2021.

663 Tao, M., Chen, L., Li, R., Wang, L., Wang, J., Wang, Z., Tang, G., and Tao, J.: Spatial oscillation of the particle
664 pollution in eastern China during winter: Implications for regional air quality and climate. *Atmos. Environ.*,
665 144, 100–110, <https://doi.org/10.1016/j.atmosenv.2016.08.049>, 2016.

666 Wang, H., Kumar, A., Murtugudde, R., Narapsetty, B., and Seip, K. L.: Covariations between the Indian Ocean
667 dipole and ENSO: a modeling study. *Clim. Dynam.*, 53, 5743–5761,
668 <https://doi.org/10.1007/s00382-019-04895-x>, 2019.

669 Wang, J., Lu, X., Yan, Y., Zhou, L., and Ma, W.: Spatiotemporal characteristics of PM_{2.5} concentration in the
670 Yangtze River Delta urban agglomeration, China on the application of big data and wavelet analysis. *Science*
671 *of the Total Environment*, 724, 138134, <https://doi.org/10.1016/j.scitotenv.2020.138134>, 2020.

672 Wang, X., Zhang, R., Tan, Y., and Yu, W.: Dominant synoptic patterns associated with the decay process of PM_{2.5}
673 pollution episodes around Beijing. *Atmos. Chem. Phys.*, 21, 2491–2508,
674 <https://doi.org/10.5194/acp-21-2491-2021>, 2021.

675 Weare, B. C. and Nasstrom, J. S.: Examples of extended empirical orthogonal function analyses. *Mon. Wea. Rev.*,
676 110, 481–485, [https://doi.org/10.1175/1520-0493\(1982\)110<0481:EOEEOF>2.0.CO;2](https://doi.org/10.1175/1520-0493(1982)110<0481:EOEEOF>2.0.CO;2), 1982.

677 Wu, B., and Wang, J.: Winter Arctic oscillation, Siberian High and EAWM, *Geophys. Res. Lett.*, 29, 1897,
678 <https://doi.org/10.1029/2002gl015373>, 2002.

679 Wu, D., Zhao, S., Li, J., and Wang, W.: Influences of atmospheric intraseasonal oscillation in mid–high latitudes on
680 winter haze pollution over the Beijing-Tianjin-Hebei region. *Int. J. Climatol.*, 43, 3173–3188,
681 <https://doi.org/10.1002/joc.8023>, 2023.

682 Wu, G., Li, Z., Fu, C., Zhang, X., and Huang, R.: Advances in studying interactions between aerosols and
683 monsoon in China. *Sci. China. Earth. Sci.*, 59, 1–16, <https://doi.org/10.1007/s11430-015-5198-z>, 2016.

684 Wu, X., He, S., Guo, J., and Sun, W.: A multi-scale periodic study of PM_{2.5} concentration in the Yangtze River
685 Delta of China based on Empirical Mode Decomposition-Wavelet Analysis, *China. Journal of Cleaner*

686 Production, 281, 124853, <https://doi.org/10.1016/j.jclepro.2020.124853>, 2021.

687 Xu, C., Ma, Y., Panday, A., Cong, Z., Yang, K., Zhu, Z., Wang, J., Amatya, P. M., and Zhao, L.: Similarities and
688 differences of aerosol optical properties between southern and northern sides of the Himalayas. *Atmos. Chem.*
689 *Phys.*, 14, 3133–3149, <https://doi.org/10.5194/acp-14-3133-2014>, 2014.

690 Xu, X., Zhao, T., Liu, F., Gong, S. L., Kristovich, D., Lu, C., Guo, Y., Cheng, X., Wang, Y., and Ding, G.: Climate
691 modulation of the Tibetan Plateau on haze in China. *Atmos. Chem. Phys.*, 16, 1365–1375,
692 <https://doi.org/10.5194/acp-16-1365-2016>, 2016.

693 Yang, Q., Zhao, T., Bai, Y., Wei, J., Sun, X., Tian, Z., Hu, J., Ma, X., Luo, Y., Fu, W., and Yang, K.: Interannual
694 variations in ozone pollution with a dipole structure over Eastern China associated with springtime thermal
695 forcing over the Tibetan Plateau. *Sci. Total Environ.*, 923, 171527,
696 <https://doi.org/10.1016/j.scitotenv.2024.171527>, 2024a.

697 Yang, S., Liu, Y., Zhu, Z., and Qi, Y.: Influence of the mid-high-latitude Eurasian ISO on PM_{2.5} concentration
698 anomaly in North China during boreal winter. *Clim. Dynam.*, 62, 2455–2474,
699 <https://doi.org/10.1007/s00382-023-07033-w>, 2024b.

700 Yang, W., Li, J., Wang, Z., Wang, L., Dao, X., Zhu, L., Pan, X., Li, Y., Sun, Y., Ma, S., Wang, W., Chen, X., and
701 Wu, J.: Source apportionment of PM_{2.5} in the most polluted Central Plains Economic Region in China:
702 Implications for joint prevention and control of atmospheric pollution, *J. Clean. Prod.*, 283, 124557,
703 <https://doi.org/10.1016/j.jclepro.2020.124557>, 2021a.

704 Yang, Y., Zhou, Y., Li, K., Wang, H., Ren, L., Zeng, L., Li, H., Wang, P., Li, B., and Liao, H.: Atmospheric
705 circulation patterns conducive to severe haze in eastern China have shifted under climate change. *Geophys.*
706 *Res. Lett.*, 48, e2021GL095011, <https://doi.org/10.1029/2021gl095011>, 2021b.

707 Yu, C., Zhao, T., Bai, Y., Zhang, L., Kong, S., Yu, X., He, J., Cui, C., Yang, J., You, Y., Ma, G., Wu, M., and Chang,
708 J.: Heavy air pollution with a unique “non-stagnant” atmospheric boundary layer in the Yangtze River middle
709 basin aggravated by regional transport of PM_{2.5} over China. *Atmos. Chem. Phys.*, 20, 7217–7230,
710 <https://doi.org/10.5194/acp-20-7217-2020>, 2020.

711 Zhang, Q., Zheng, Y., Tong, D., Shao, M., Wang, S., Zhang, Y., Xu, X., Wang, J., He, H., Liu, W., Ding, Y., Lei, Y.,
712 Li, J., Wang, Z., Zhang, X., Wang, Y., Cheng, J., Liu, Y., Shi, Q., Yan, L., Geng, G., Hong, C., Li, M., Liu, F.,
713 Zheng, B., Cao, J., Ding, A., Gao, J., Fu, Q., Huo, J., Liu, B., Liu, Z., Yang, F., He, K., and Hao, J.: Drivers of
714 improved PM_{2.5} air quality in China from 2013 to 2017, *P. Natl. Acad. Sci. USA*, 116, 24463–24469,
715 <https://doi.org/10.1073/pnas.1907956116>, 2019.

716 Zhang, X., Wang, Y., Niu, T., Zhang, X., Gong, S., Zhang, Y., and Sun, J.: Atmospheric aerosol compositions in
717 China: Spatial/temporal variability, chemical signature, regional haze distribution and comparisons with global
718 aerosols. *Atmos. Chem. Phys.*, 12, 779–799, <https://doi.org/10.5194/acp-12-779-2012>, 2012.

740 Zhang, X., Xu, X., Ding, Y., Liu, Y., Zhang, H., Wang, Y., and Zhong, J.: The impact of meteorological changes
741 from 2013 to 2017 on PM_{2.5} mass reduction in key regions in China. *Sci. China Earth Sci.*, 62, 1885–1902,
742 <https://doi.org/10.1007/s11430-019-9343-3>, 2019.

743 Zhang, Y., Ding, A., Mao, H., Nie, W., Zhou, D., Liu, L., Huang, X., and Fu, C.: Impact of synoptic weather
744 patterns and inter-decadal climate variability on air quality in the North China Plain during 1980–2013. *Atmos.*
745 *Environ.*, 124, 119–128, <https://doi.org/10.1016/j.atmosenv.2015.05.063>, 2016.

746 Zhao, S., Feng, T., Tie, X., Dai, W., Zhou, J., Long, X., Li, G., and Cao, J.: Short-term weather patterns modulate
747 air quality in eastern China during 2015–2016 winter. *J. Geophys. Res.-Atmos.*, 124, 986–1002,
748 <https://doi.org/10.1029/2018jd029409>, 2019.

749 Zheng, B., Tong, D., Li, M., Liu, F., Hong, C., Geng, G., Li, H., Li, X., Peng, L., Qi, J., Yan, L., Zhang, Y., Zhao,
750 H., Zheng, Y., He, K., and Zhang, Q.: Trends in China’s anthropogenic emissions since 2010 as the

751 consequence of clean air actions. *Atmos. Chem. Phys.*, 18, 14095–14111,
752 <https://doi.org/10.5194/acp-18-14095-2018>, 2018a.

753 Zheng, Z., Ren, G., Wang, H., Dou, J., Gao, Z., Duan, C., Li, Y., Ngarukiyimana, J. P., Zhao, C., Cao, C., Jiang, M.,
754 and Yang, Y.: Relationship between fine-particle pollution and the urban heat island in Beijing, China:
755 observational evidence. *Bound-Lay. Meteorol.*, 169, 93–113, <https://doi.org/10.1007/s10546-018-0362-6>,
756 2018b.

757 Zhong, J., Zhang, X., Dong, Y., Wang, Y., Liu, C., Wang, J., Zhang, Y., and Che, H.: Feedback effects of
758 boundary-layer meteorological factors on cumulative explosive growth of PM_{2.5} during winter heavy pollution
759 episodes in Beijing from 2013 to 2016. *Atmos. Chem. Phys.*, 18, 247–258,
760 <https://doi.org/10.5194/acp-18-247-2018>, 2019.

761 Zhu, W., Xu, X., Zheng, J., Yan, P., Wang, Y., and Cai, W.: The characteristics of abnormal wintertime pollution
762 events in the Jing-Jin-Ji region and its relationships with meteorological factors. *Sci. Total Environ.*, 626, 887–
763 898, <https://doi.org/10.1016/j.scitotenv.2018.01.083>, 2018.